frontiers | Frontiers in Materials

TYPE Original Research
PUBLISHED 18 April 2024
DOI 10.3389/fmats.2024.1388695

OPEN ACCESS

EDITED BY
Farzad Nasirpouri,
Sahand University of Technology, Iran

REVIEWED BY
Naeimeh Sadat Peighambardoust,
Koç University, Türkiye
Ali Saad,
Aarhus University, Denmark

*CORRESPONDENCE
Fan Li,
vanadiumli@bjut.edu.cn
Yong Yan,
yong.yan@bjut.edu.cn
Ying-Jie Feng,
fengyj.bjhy@sinopec.com

RECEIVED 20 February 2024
ACCEPTED 02 April 2024
PUBLISHED 18 April 2024

CITATION
Li X-Y, Xu L-C, Wang Y, Yan Y, Feng Y-J and Li F (2024), Highly defective NiFeV layered triple hydroxide with enhanced electrocatalytic activity and stability for oxygen evolution reaction.
Front. Mater. 11:1388695.
doi: 10.3389/fmats.2024.1388695

Highly defective NiFeV layered triple hydroxide with enhanced electrocatalytic activity and stability for oxygen evolution reaction

Xi-Yuan Li[1], Lin-Cheng Xu[1], Yue Wang[1], Yong Yan[2]*, Ying-Jie Feng[3]* and Fan Li[1]*

[1]Beijing Key Laboratory for Catalysis and Separation, Department of Chemical Engineering, College of Materials Science and Engineering, Beijing University of Technology, Beijing, China, [2]Beijing Key Laboratory for Catalysis and Separation, Department of Chemistry, Faculty of Chemistry and Life Science, Beijing University of Technology, Beijing, China, [3]Department of Catalytic Science, SINOPEC (Beijing) Research Institute of Chemical Industry Co., Ltd., Beijing, China

Oxygen evolution reaction (OER) is one of the most important components of various electrochemical systems such as water splitting, metal air batteries, and carbon dioxide reduction. However, the four-electron process of OER suffers from intrinsically sluggish kinetics, which contributes to significant overpotential in the electrochemical system. Herein, highly defective NiFeV layered triple hydroxide (LTH) catalyst was efficiently prepared using a one-step hydrothermal method. The crystal structure, electronic structure, and surface composition of NiFeV LTH were characterized by X-ray diffraction and photoelectron spectroscopy. Moreover, NiFeV LTH demonstrated a superior OER catalytic performance with-low overpotential (158 mV @10 $mA{\cdot}cm^{-2}$), related small Tafel slope (102.3 $mV{\cdot}dec^{-1}$), and long-term stability at a high current density of 100 $mA{\cdot}cm^{-2}$. *In situ* Raman spectroscopy was applied to investigate the surface reconstruction during the OER process. It is revealed that Ni species were the most active sites at low overpotential, with the potential increasing subsequently Fe and V gradually participates in the catalytic reaction, the Fe and Ni species as OER catalytic active sites lead to the excellent OER catalytic activity of NiFeV LTH, and inhibited the further dissolution of high-valence NiOOH at high overpotential. The mechanism induced the outstanding activity and stability at high current densities in NiFeV LTH system. Dissolution of vanadium excited the active sites of NiFeV LTH synthesized by hydrothermal method which promoted both activity and stability, while the changes of surface species at different OER potentials were detected by *in situ* Raman spectroscopy.

KEYWORDS

oxygen evolution reaction, layered triple hydroxide, in situ Raman spectroscopy, high stability, NiFeV LTH

Introduction

Hydrogen production from water spitting plays an important role in the development of renewable energy technology. In the hydrogen production reaction, the oxygen evolution reaction (OER) and hydrogen evolution reaction (HER) occur at the anode and cathode respectively. In the OER reaction, which is a four-electron process, the path of reaction is more complex compared with HER and contributes significantly to the overpotential (Suen et al., 2017). Electrocatalysts for the OER reaction must combine both activity and stability at high oxidation potentials. The noble metal-based catalysts, represented by Ru and Ir, are limited in resources, which hinders their large-scale application. Meanwhile, Ru is especially relatively unstable and tends to undergo dissolution at the oxygen evolution potential, leading to material consumption (Schalenbach et al., 2018; Zeng et al., 2022). Transition metal-based electrocatalysts such as Fe Co Ni-based electrocatalysts in fourth cycle have sufficiently high stability OER performance under alkaline conditions (Jamesh and Sun, 2018).

Among numerous transition metal-based electrocatalysts, the LDH-type catalysts are a potential class of OER electrocatalysts. In the LDH-type OER electrocatalysts, metal ions in different valence states forming a layered skeleton, which was conducive to the electrocatalytic reaction, and the adjustability of the insertion layer and composition improve oxygen precipitation performance (Karmakar et al., 2021). Among the LDH-type catalysts, the OER performance of NiFe LDH was more prominent, in which both Fe and Ni possessed OER activity and function as cocatalysts (Chen et al., 2015; Shin et al., 2018), whereas the LDH phase exhibits thermodynamic stability at the OER potential (Peng et al., 2021). NiFe LDH has numerous modification methods, including regulating the concentration ratio of metal ions, adjusting components, adding NH_4F to regulate morphology, and adjusting anions during intercalation (Chen et al., 2019; Zhong et al., 2019; Huang et al., 2021; Suppaso et al., 2021). In addition, doping with other metal ions can also help to improve the OER performance of LDH. For example, Guo et al. demonstrated that introducing Zn into the NiFe LDH lattice can promote self-reconstruction and form higher density active sites through the dissolution of zinc ions in the electrolyte (Guo et al., 2023). Vanadium is also a doping element that is easy to coprecipitate with Fe and can form stable LDH with Ni. Its stable valence is high, which is conducive to the improvement of electrical conductivity of LDH under a mixed valence state (Fan et al., 2016; Fan et al., 2017). Other studies have shown that the introduction of V facilitates lattice fragmentation in LDH, which is conducive to the enhancement of activity (Fan et al., 2020), and that the rapid dissolution of vanadium under alkaline conditions under open cicuit potentials (OCP) facilitates the exposure of the active sites and forms a stable and dense layer with catalytic activity that reduces the dissolution of the active components (Adamson et al., 2021). Some researchers have found that the dissolution of some metal components such as Zn, Al, Mo, and V during the OER process can stimulate defects from OER active sites, which is a new method for *in situ* optimization of LDH catalytic material performance (Wang et al., 2018; Fan et al., 2020; Xu et al., 2020). LDH-type catalysts still suffer from poor electronic conductivity and exhibit a certain gap in OER performance compared with noble metal-based catalysts. Research on the OER activity mechanism and the design criteria for improving OER performance after doping with other elements are still insufficient.

In this work, an OER catalyst of NiFeV layered triple hydroxide (LTH) ternary was synthesized using a hydrothermal method, which demonstrated a superior OER performance. Dissolving of vanadium excited the OER active sites promoted both activity and stability. *In situ* Raman test indicated that the introduction of vanadium inhibited the further dissolution of high-valence species and reduced the amount of Ni species to convert to a high-valence state, which provided a basis for the design and improvement of activity and stability for LDH-type OER catalysts. The above results can provide new insights for designing and constructing high-performance LTH catalytic materials.

Experimental section

Chemicals: $FeCl_3{\cdot}6H_2O$ and Fe $(NO_3)_3$, were purchased from Macklin. $VOSO_4$, urea $(CO(NH_2)_2)$, H_3BO_3, and potassium hydroxide (KOH, 85%) were acquired from J&K Scientific. Ni foam was acquired from Alfa Aesar. All reagents were of analytical grade and used as received without further purification.

Synthesis of the catalysts

Synthesis of NiFeV LTHs: $FeCl_3{\cdot}6H_2O$ (0.65 mmol), $VOSO_4{\cdot}5H_2O$ (0.65 mmol), H_3BO_3 (8 mmol), and $CO(NH_2)_2$ (2 mmol) were dissolved in 17 mL of distilled water and stirred to form a clear solution. Nickel foam (NF, about 3 cm × 3 cm) was carefully cleaned with diluted HCl solution and absolute ethanol in an ultrasound bath for 30 min each time to remove the surface NiO layer, and then cleaned using deionized water. NF and the above solution were transferred to a 40 - mL Teflon-lined stainless steel autoclave. The catalyst was synthesized by hydrothermal heating at 120 °C for 24 h, and then cooled to room temperature naturally. A brown thin film was formed on the metal substrate, and the products were cleaned with deionized water/ethanol and dried at room temperature for 24 h.

NiFe LDHs: NiFe LDHs were synthesized using the same method as that of NiFeV LDH without adding $VOSO_4$. NiV LDHs were synthesized using the same method without the addition of an Fe source.

Materials characterization

The size and morphology of the samples were characterized using a field-emission scanning electron microscope (SEM, HITACHI su8000) operating at 20 kV. High-resolution transmission electron microscopy (HR-TEM) measurements were carried out using a JEOL JEM 2100 system operating at 200 kV. Energy dispersive spectrometer (INCA) as attachment of SEM and TEM. X-ray powder diffraction (XRD) patterns were recorded on an X-ray diffractometer (Rigaku D/max 2,500) with Cu Kα radiation (40 kV, 30 mA, λ = 1.5418 Å) at a scan rate of 10° min^{-1} in the 2θ range from 10° to 80°. Valence state analysis of the surface was conducted using

X-ray photoelectron spectroscopy (XPS, ESCALAB 250Xi) with an Al Kα radiation source. The elemental composition of the LDH and LTH catalysts was also investigated using inductively coupled plasma optical emission spectrometry (ICP-OES, Optima 8,300, PerkinElmer of America).

In situ Raman spectroscopy

These experiments were performed in a customized three-electrode *in situ* Raman cell (Aida K004). A reference electrode (Ag/AgCl, in saturated KCl solution) and a counter electrode (silver wire) were used. A Donghua electrochemical workstation (DH7000C 4 China) was used to perform OER electrolysis processes. The 1.0 M KOH electrolyte was delivered into the cell using a peristaltic pump. *In situ* Raman measurements were performed using confocal Raman spectroscopy (Invia Raman microscope, Renishaw) with a 532-nm wavelength laser, an L5×0 objective, a CCD detector, and a laser power of ~100%. The exposure time was set to 10 s for each spectrum with an accumulation time of 1. The spectrum was calibrated before acquisition on the basis of the wavenumber of silicon, 520 ± 0.5 cm^{-1}. For a typical measurement, 20 cycles of cyclic voltammetry (CV) between 0 and 1.7 V vs. RHE was first performed to obtain a stable current response. Raman spectra were collected using the chronoamperometry (CA) process at different potentials with a testing exposure time of 10 s.

Electrochemical measurements

A three-electrode system was used in this study. NF loaded with the catalyst was used as the working electrode, with an Hg/HgO reference electrode and a carbon rod counter electrode. CV, linear sweep voltammetry (LSV), electrochemical impedance spectroscopy (EIS, frequency range: 10^5–10^{-1} Hz, amplitude: ±5 mV), CA and chronopotentiometry (CP) were performed to evaluate the electrocatalytic performance. Electrochemical tests were performed in 1 M of KOH solution saturated with argon for activation and then saturated with oxygen for electrochemical measurement. All electrochemical tests were performed using a Metrohm Autolab PGSTAT302N electrochemical workstation without iR compensation. On the basis of the LSV curves, OER, the overpotential η, and the log$j$ of the current density was plotted according to the following equation (Shinagawa et al., 2015), and the resulting b is the value of the Tafel slope.

Equation (Shinagawa et al., 2015)

$$\eta = a + b \log j$$

where η defines the overpotential (V), j denotes the current density (mA·cm^{-2}), and a and b are constant. The electrochemical active surface area (ECSA) of the catalyst can be obtained from the double layer capacitance (C_{dl}) which calculated from the rectangular CV in the region excluding any faradic process (Saad et al., 2022a), and the ECSA is measured as ECSA = C_{dl}/C_s (C_s = 0.040 mF·cm^2 in 1M KOH) (Saad et al., 2023).

Results and discussion

NiFeV LTH was synthesized using the hydrothermal method. SEM image shows that NiFeV LTH was lamellar and formed a film on the NF substrate, as shown in Figure 1A. The SEM-EDS test on the as prepared sample shows that the Fe, V, Ni, and O elements on the surface were evenly distributed (Supplementary Figure S1). The lamellar morphology was observed by TEM (Figure 1B) also. Because the thickness of the thin layer formed by NiFeV LTH on the surface of the NF is small, only the Ni peak appears in the XRD spectrum (Yang et al., 2019), as shown in Supplementary Figure S1A. This is because NiFeV LTH only exists on the surface of NF with a low loading amount, and no obvious signal of LTH from XRD. Therefore, the peeled powder on the surface was tested, the diffraction peaks of the powder sample at 11.6°, 23.5°, 34.6°, and 35.7° were observed using the XRD (Fig. S2b), and the planes of (003), (006), (101), and (012) are well agreed upon and can be indexed as standard NiFe LDH (JCPDS No. 40–0215). ICP-OES testing was conducted to determine the loading of the metal elements, the results are listed in Supplementary Table S1. High Angle Angular Dark Field-Scanning Transmission Electron Microscopy (HAADF-STEM) images and corresponding EDS element mapping of the samples (Figures 1B–E) indicate that Ni, Fe, V, and O are uniformly distributed in NiFeV LTH, and the atomic ratio from TEM-EDS (Supplementary Table S2) is consistent with the ICP-OES result (Supplementary Table S1) and SEM-EDS (Supplementary Table S3). NiFeV LTH does not exhibit significant phase segregation during growth. The loading amount (3.2 mg·cm^{-2}) of NiFeV LTH on the surface of the NF was calculated by combining the ICP-OES, EDS, and the general formula $[M_{1-x}{}^{II}M_x{}^{III}(OH)_2]^{Z+}(A^{n-})_{z/n}\cdot 2H_2O$ (M^{II}: divalent metals, M^{III}: trivalent metals, A^{n-}: the interlayer anion) (Wang et al., 2018). The valence state of the surface elements would be examed by XPS.

XPS testing was performed on the as prepared NiFeV LTH and NiFe LDH samples. A typical XPS survey spectrum is shown in Supplementary Figure S3, which depicts the presence of Ni, Fe, V, and O elements on the surface of NiFeV LTH samples, whereas only Ni, Fe, and O are present in the NiFe LDH samples. The high-resolution deconvoluted XPS spectra of Fe 2p and Ni 2p are shown in Figures 2A, B, which indicate that the valence states of iron and nickel in NiFeV LTH and NiFe LDH are mainly +2 and +3 both, and a small amount of metallic nickel may be derived from the exposed NF during sample preparation. The XPS spectrum of O 1s deconvolve into four peaks at 529.9 eV, 530.8 eV, 531.9 eV, and 533.1 eV (Figure 2C), which are assigned for O^{2-}, OH^-, -OOH, and adsorbed water, respectively (Sagar et al., 2022). According to the XPS spectrum of V 2p, vanadium on the surface of NiFeV LTH is in the mixed valence state of V^{3+} (516.1 eV) and V^{4+} (517.2 eV) (Qian et al., 2023) with a binding energy blueshift (Silversmit et al., 2004), which may lead to a decrease in the crystallinity of NiFeV LTH compared with NiFe LDH, as reflected in the XRD pattern results (Fig. S1b). The fitting results (Supplementary Tables S4, S5) show that the proportion of Fe^{3+}among surface Fe species in NiFeV LTH is reduced compared with that in NiFe LDH, whereas the XPS spectrum of V 2p in Figure 2D displays some vanadium with a valence state +4 higher than trivalent. The reduction of Fe^{3+} may be related to V species with a higher charge density than Fe or Ni species

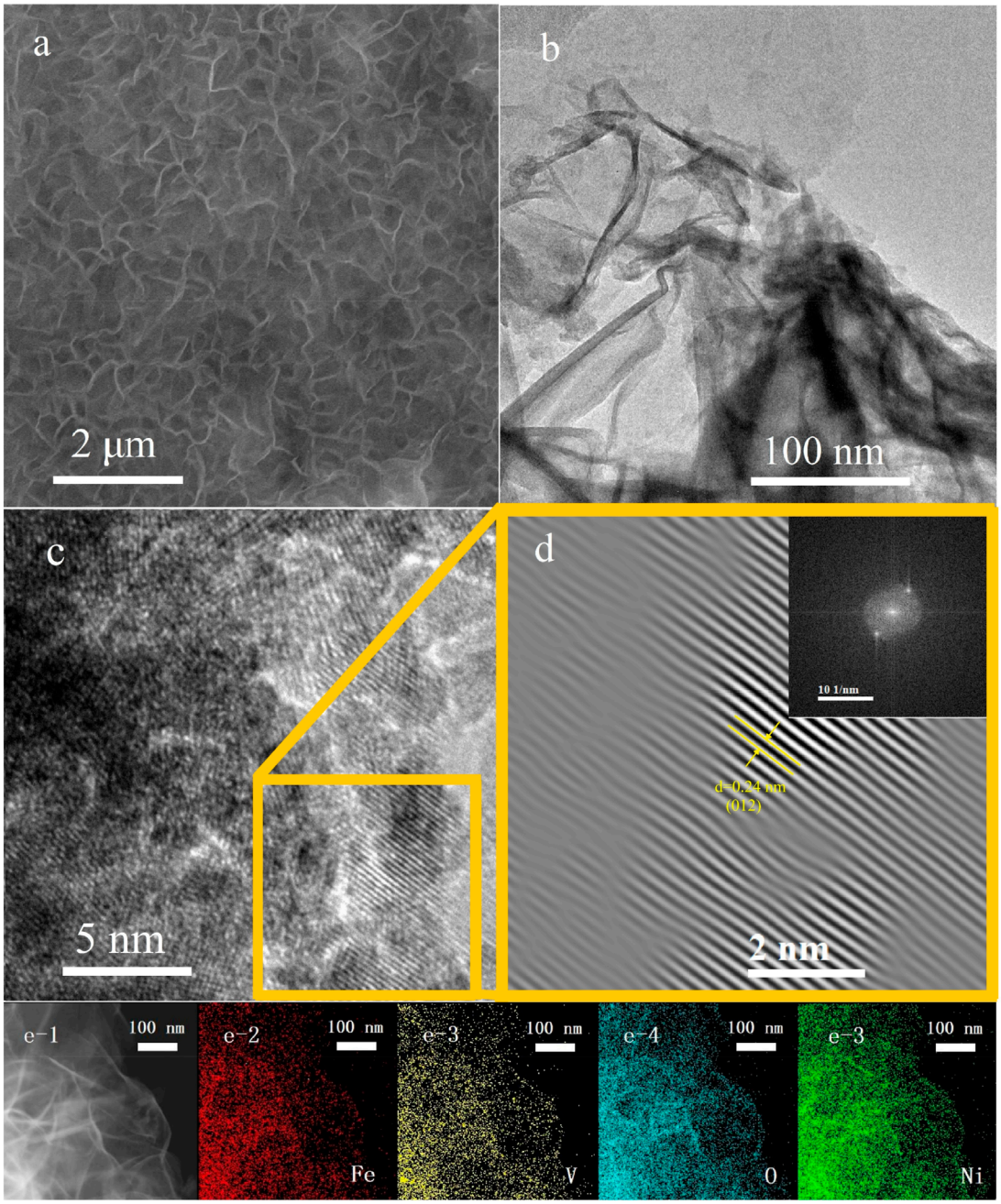

FIGURE 1
(A) SEM image; **(B)** TEM image; **(C)** HR-TEM images, **(D)** enlarged part of **(C)**, and **(E)** HAADF-STEM and EDS mapping of NiFeV LTH.

entering the lattice and occupying high-valence example positions (Li et al., 2018). Figure 2B shows the high-resolution deconvoluted XPS spectra of Ni 2p. The fitted peak positions at 855.4 eV and 856.2 eV were assigned to Ni^{2+} and Ni^{3+}, respectively (Sagar et al., 2022), and the fitting results are shown in Supplementary Table S4. It found that the Ni element in NiFeV LTH had a higher proportion of Ni^{3+}specy compared with NiFe LDH, and positive shift of Fe^{3+} and Ni^{3+} peaks in NiFeV LTH compared to NiFe LTH. This indicates a decrease in the electron density in $Fe^{3+}$and Ni^{3+} (indicating a transformation from $Fe^{2+}$and Ni^{2+} to $Fe^{3+}$and Ni^{3+}), which may be related to the high-valence V enter in the lattice. The oxidation ability of the trivalent nickel is higher than that of trivalent iron, and the entry of high-valent vanadium hinders electron transfer during the LTH growth process, keeping nickel in a higher valence state and iron in a lower valence state. This may lead to the formation of more defective structures and improve conductivity, which has a positive impact on the OER performance of the material (Li et al., 2018).

Figure 3A shows the electrocatalytic activity tests of NiFeV LTH, NiFe LDH, NiV LDH, and Ni foam (NF) in a 1M KOH solution. In the OER LSV test, the oxidation peaks of NF and

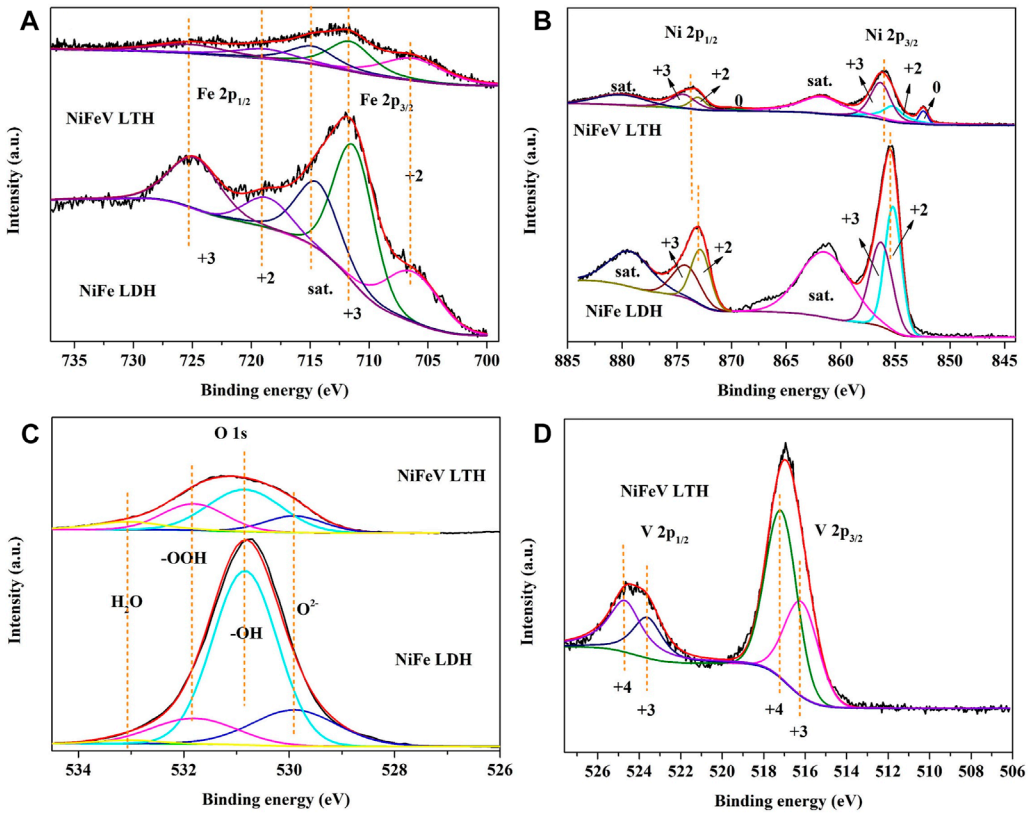

FIGURE 2
XPS spectra of NiFe LDH and NiFeV LTH **(A)** Fe, **(B)** Ni, **(C)** O, and **(D)** V.

NiV LDH at 1.4 V vs. RHE are surface species oxidation peaks (Saad et al., 2022b), the oxidation peaks occur due to NF and NiV LDH exhibited high OER onset potential, while NiFe LDH and NiFeV LTH have a lower OER onset potential, the oxidation peak around 1.4 V was covered by the OER current. NiFeV LTH exhibited superior OER electrocatalytic performance (158 mV @10 mA·cm^{-2}, 350 mV @100 mA cm^{-2}). The performances are better than those of NiFe LDH (202 mV @10 mA·cm^{-2}, 440 mV @100 mA·cm^{-2}) respectively. The Tafel slopes were used to evaluate the OER kinetics of these active materials. NiFeV LTH exhibits the lowest Tafel slope (102.3 mV·dec^{-1}), which is lower than that of NiFe LDH (197.4 mV·dec^{-1}), NiV LDH (165.2 mV·dec^{-1}), and NF (254.4 mV·dec^{-1}). NiFeV LTH exhibited efficient OER kinetics. NiFeV LTH has better activity compared to RuO_2 (248 mV @10 mA·cm^{-2}, 117 mV·dec^{-1}) at the same loading amounts also (Supplementary Figure S4). The loading amount of NiFeV LTH and RuO_2 were listed in Supplementary Table S8. ECSA were investigated to determination of specific electrocatalytic activity. The C_{dl} results (Supplementary Figure S5) show that the C_{dl} of NiFeV LTH was larger than NiFe LDH, this indicating that NiFeV LTH with a large accessible surface area and high catalytic activity. the ECSAs of different samples were calculated and the results were listed in Supplementary Table S9. The OER polarization curves of NiFeV LTH and NiFe LDH were normalized to the ECSA (Fig. S5d) the normalized results show that NiFeV LTH has comparable intrinsic activity to NiFe LDH at low overpotential, and the current density of NiFeV LTH lower than NiFe LDH at high overpotential. Diffusion might be the rate-determining step at high overpotential. It is speculated that the entries of high-valence V into the lattice may facilitate the formation of highly active Ni and Fe species. EIS testing was performed at 1.53 V vs. RHE of the synthesized material the results show in Figure 3C, and the fitting results are listed in Supplementary Table S6. The solution resistance is 1.54 Ω for NiFeV LTH, 1.96 Ω for NiFe LDH, 1.16 Ω for NiV LDH, and 2.08 Ω for NF. Because of the two interfaces (NF the interfaces between support and catalytic material and the interfaces between catalytic material and solution), the Nyquist plots show a double arc; therefore, in the fitted circuit, the obtained total resistance includes R_1 (coating resistance) and R_{ct} (charge transfer resistance), which correspond to the process of charge transfer from the NF to the catalytic material (R_1) and from electrolyte to the catalytic material (R_{ct}), respectively (Chandrasekaran et al., 2022). The magnitude of the total resistance indicates the difficulty of the transfer processes. A lower total resistance indicates that the material has higher conductivity and better OER electrocatalytic activity (Chandrasekaran et al., 2022). The fitting results show that under the same overpotential (300 mV), NiFeV LTH has the smallest R_1, R_{ct}, and observed total resistance among all tested samples. It indicated NiFeV LTH with the best conductivity and highest electrocatalytic activity.

Stability is important for electrocatalytic performance; thus, a CP test was carried to measure the OER stability of the materials. The CP tests (@100 mA·cm^{-2}, 16 h) were performed on NiFe LDH,

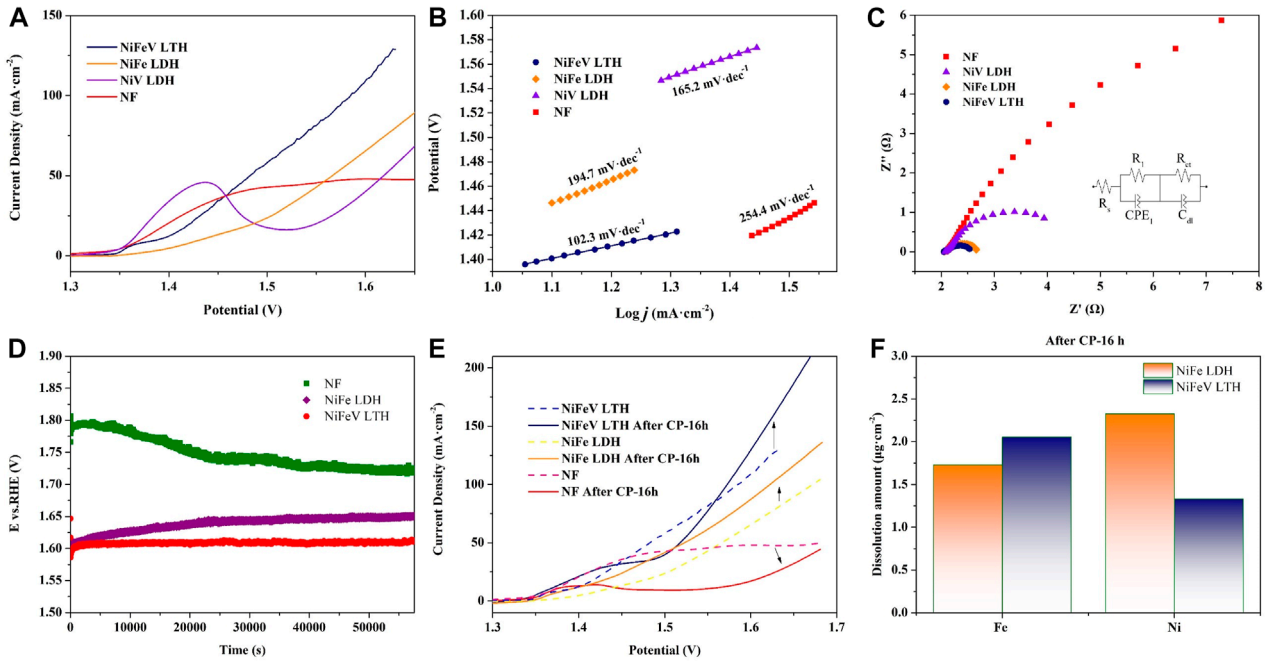

FIGURE 3
(A) OER polarization curves, **(B)** Tafel slopes, **(C)** Nyquist plots of NiFeV LTH, NiFe LDH, NiV LDH, and NF, the inset was the equivalent circuit, **(D)** CP curves, **(E)** comparation of OER polarization curves before and after CP testing, and **(F)** dissolution of nickel and iron after CP testing for NiFeV LTH and NiFe LDH.

NiFeV LTH, and NF, and the test results are shown in Figure 3D. In the CP test, the voltage retention rates of NiFe LDH and NiFeV LTH were 86.5% and 96.2%, respectively. The overpotential of NF decreased because of the presence of a hydroxyl oxide layer under high potential, but it was still much higher than those of NiFe LDH and NiFeV LTH. Results of CP test show that NiFeV LTH has excellent stability at a current density of 100 $mA{\cdot}cm^{-2}$. After CP testing, there was no significant decrease of current density at same overpotential for NiFe LDH and NiFeV LTH (Figure 3E). The increase in activity (current density) under high overpotential may be related to surface reconstruction with excitation of the Fe and Ni active sites. Further investigation was conducted on the dissolved Fe and Ni ions of NiFe LDH and NiFeV LTH before and after 16 h CP testing (Figure 3F). The ICP-OES results show that the amounts of dissolved Ni and Fe ion of the two materials were almost equivalent. Continue the CP test to 20h, The dissolution of vanadium is relatively abundant compared with nickel and iron, as listed in Supplementary Table S7, which may excite a large number of coordination unsaturated active sites. The amount of Fe and Ni species of CP-20 h decreased in the electrolyte compare to CP-16 h may be related to the dissolution precipitation equilibrium in alkaline electrolytes. In a long-term CP (72 h) test, the voltage retention rates of NiFeV LTH was 93.2%, respectively (Fig. S6a), and there was no significant decrease in the electrocatalytic performance NiFeV LTH after CP (72 h) testing (Fig. S6b), NiFeV LTH performs outstanding OER stability at high current density. CA test was also carried for the sample. Supplementary Figures S7-S9 show the CA test results at 1.58 V vs. RHE, as well as the XPS and SEM images of the active samples and the samples after CA test. The results show that the surface of NiFeV LTH has undergone reconstruction, and vanadium mainly dissolved during the activation process. It speculated that the higher activity and stability of NiFeV LTH compared with NiFe LDH might be related to the dissolution of V.

To further explore the OER electrocatalytic mechanism of NiFeV LTH, *in situ* Raman spectroscopy was used to detect the intermediates on the surface of the electrode with a change in potential. NiFe LDH and NiFeV LTH were tested separately, and Figures 4A, B show the *in-situ* Raman spectra of NiFeV LTH and NiFe LDH as the potential gradually increases from the OCP, to detect the kinetic process of interface evolution. At high overpotentials, oxygen bubbles interfere with laser focusing, resulting in an upper limit potential of 1.53 V vs. RHE. In Raman spectroscopy, the peaks around 450 $cm^{-1}$and 520 cm^{-1} represents the Ni-O bonds (Tang et al., 2020), and the peaks around 470 and 555 cm^{-1} were attributed to, e.g., bending vibration and the A_{1g} stretching vibration of Ni-O bonds in NiOOH (Zhu et al., 2019). The peaks around 320 and 690 cm^{-1} represent the brucite structure in LDHs and the symmetric stretching of the A_{1g} symmetry of $NiFe_2O_4$ (Tang et al., 2020; 2022). The broad peak from 760 to 950 cm^{-1} represents the V-O peak (Shvets et al., 2019; Qian et al., 2023) and the 1055 cm^{-1} peak derived from the carbonate ions in the intercalation (Elena et al., 2014). In the Raman spectrum of NiFeV LTH, the Ni-O bimodal peak of 448 and 521 cm^{-1} blueshifted to 469 and 555 cm^{-1} in the potential range from 1.33 to 1.43 V vs. RHE, indicating a transition of Ni species toward higher valence states, which is related to the generation of high OER active phases. The same blue shift in NiFe LDH at the same potentials was not detected, indicating that high OER active species are generated much easier in NiFeV LTH, which may denote that more tetravalent Fe and Ni species with high OER

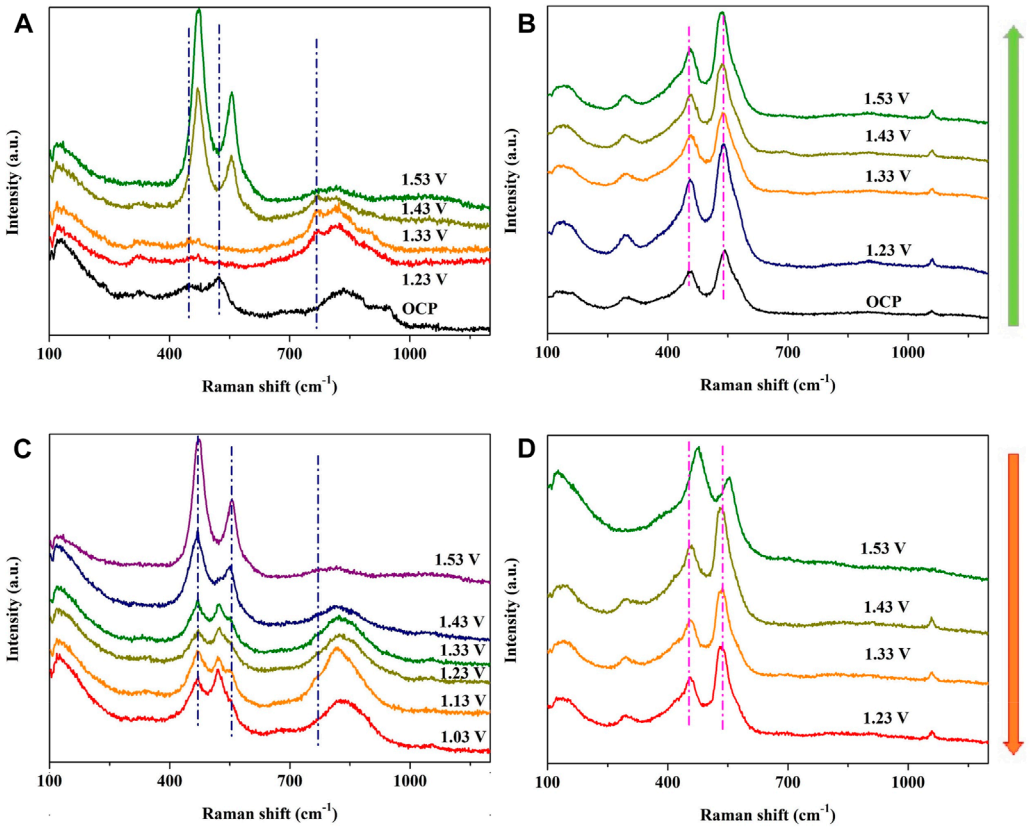

FIGURE 4
In situ Raman spectra of **(A)** NiFeV LTH and **(B)** NiFe LDH for the OER process with an interval voltage of 0.1 V, and the inverse scanning of **(C)** NiFeV LTH and **(D)** NiFe LDH.

activity form on the surface of NiFeV LTH and participate in the reaction (Chen et al., 2015; Shin et al., 2018), leading to higher catalytic activity compared with NiFe LDH. The narrow peak of V-O at 765 cm^{-1} may be related to the oxidation of vanadium, which may have led to different behaviors of the Ni and Fe species mentioned above. *In situ* Raman testing with positive scanning revealed that the potential for the generation of high-valent species on the surface of NiFeV LTH decreases with a higher blue shift than NiFe LDH, which may be related to the dissolution of surface vanadium. To determine the stability of highly active species on the surface, potential reverse scanning was performed. The polarization curves are shown in Supplementary Figure S10. The high-valent Ni species in NiFe LDH rapidly transformed into low-valent species, which was reflected by the red shift of the Ni-O peak at a potential range of 1.53–1.43 V vs. RHE. However, during the potential reverse scanning process, the V-O peak of NiFeV LTH becomes narrower compared with the positive scan, which may be related to the irreversible dissolution of high-valent vanadium. The dissolution of vanadium is beneficial for the formation of iron and nickel oxyhydroxide active defects (Adamson et al., 2021). Reports have shown that the Fe-O vibrational peak and Ni-O peak overlap relatively high, both located in the range of 455–555 cm^{-1} (Adamson et al., 2021; Tang et al., 2022). During the process of potential decrease, the double peaks near 553 and 519 cm^{-1} did not show the same red shift as NiFe LDH, which may be related to the asynchronous reduction of Ni and Fe valence states caused by the introduction of vanadium.

Further experiments were conducted on NiFeV LTH using *in situ* Raman spectroscopy after stability testing (Supplementary Figure S11). After 7 h CP testing at a current density of 100 $mA{\cdot}cm^{-2}$, strong Ni-O peaks were captured at 479 and 559 cm^{-1}, while the V-O peaks disappeared. The XPS spectra results in Supplementary Figure S8 show that $Ni^{2+}$and Ni^{3+} both shifted toward a higher binding energy compared with the pristine sample, and surface V species were significantly dissolved after long-term OER reactions, which was consistent with the Raman spectroscopy results. In Supplementary Figure S9, the SEM image shows that after a long-term reaction, the surface of the NiFeV LTH remained a layered structure, which is consistent with the high-valence Ni-O peak of NiOOH in the Raman spectrum. Therefore, NiFeV LTH has a superior OER stability because the morphology of NiFeV LTH remains stable, whereas vanadium, as a common dissolved component lead to surface reconstruction and stable active species during the OER process.

Conclusion

In summary, NF-supported NiFeV LTH was synthesized using the hydrothermal method. The obtained NiFeV LTH is a promising

OER electrocatalyst with significantly high electrochemical activity and stability. *In situ* Raman spectroscopy was used to study the surface changes of NiFe LDH and NiFeV LTH during the OER process. The shift of peaks in situ Raman spectroscopy preliminarily revealed the surface reconstruction of catalysts during the OER process. Spectral testing of the oxidation and reduction processes of NiFeV LTH and NiFe LDH during the OER process is helpful for understanding the mechanism of the OER process in LDH-type catalysts, and it provides some insights into the mechanism of improving catalyst performance by introducing other metal ion modification methods.

Data availability statement

The original contributions presented in the study are included in the article/Supplementary Material, further inquiries can be directed to the corresponding authors.

Author contributions

X-YL: Data curation, Formal Analysis, Investigation, Writing–original draft. L-CX: Formal Analysis, Investigation, Writing–review and editing. YW: Formal Analysis, Investigation, Writing–review and editing. YY: Conceptualization, Supervision, Visualization, Writing–review and editing. Y-JF: Conceptualization, Funding acquisition, Supervision, Writing–review and editing. FL: Conceptualization, Funding acquisition, Supervision, Writing–review and editing.

Funding

The author(s) declare that financial support was received for the research, authorship, and/or publication of this article. This study was supported by the National Natural Science Foundation of China (NSFC 52074016) and Sinopec research fund 122060.

Acknowledgments

The authors would like to express thanks to the National Natural Science Foundation of China (NSFC 52074016) and Sinopec research fund 122060 for their financial support.

Conflict of interest

Y-JF was employed by SINOPEC (Beijing) Research Institute of Chemical Industry Co., Ltd.

The authors declare that the research was conducted in the absence of any commercial or financial relationships that could be construed as a potential conflict of interest.

Publisher's note

Supplementary material

The Supplementary Material for this article can be found online at: https://www.frontiersin.org/articles/10.3389/fmats.2024.1388695/full#supplementary-material

References

Adamson, W., Jia, C., Li, Y., and Zhao, C. (2021). Vanadium-induced fragmentation of crystalline CoFe hydr(oxy)oxide electrocatalysts for enhanced oxygen evolution reaction. *Int. J. Hydrogen Energy* 46 (71), 35230–35238. doi:10.1016/j.ijhydene.2021.08.080

Chandrasekaran, P., Edison, T. N. J. I., and Sethuraman, M. G. (2022). Electrocatalytic study of carbon dots/Nickel iron layered double hydroxide composite for oxygen evolution reaction in alkaline medium. *Fuel* 320, 123947. doi:10.1016/j.fuel.2022.123947

Chen, J. Y. C., Dang, L., Liang, H., Bi, W., Gerken, J. B., Jin, S., et al. (2015). Operando analysis of NiFe and Fe oxyhydroxide electrocatalysts for water oxidation: detection of Fe^{4+} by mossbauer spectroscopy. *J. Am. Chem. Soc.* 137 (48), 15090–15093. doi:10.1021/jacs.5b10699

Chen, R., Hung, S., Zhou, D., Gao, J., Yang, C., Tao, H., et al. (2019). Layered structure causes bulk NiFe layered double hydroxide unstable in alkaline oxygen evolution reaction. *Adv. Mater.* 31 (41), e1903909. doi:10.1002/adma.201903909

Elena, V. T., Pavel, T. E., Larisa, V. T., Julia, V. P., Larisa, T. A., and Svetlana, V. P. (2014). "Raman spectroscopy for monitoring of organic and mineral structure of bone grafts," in Paper presented at the Proceedings of SPIE, 1000 20TH ST, PO BOX 10, BELLINGHAM, WA 98227-0010 USA, SPIE.

Fan, K., Chen, H., Ji, Y., Huang, H., Claesson, P. M., Daniel, Q., et al. (2016). Nickel-vanadium monolayer double hydroxide for efficient electrochemical water oxidation. *Nat. Commun.* 7, 11981. doi:10.1038/ncomms11981

Fan, K., Ji, Y., Zou, H., Zhang, J., Zhu, B., Chen, H., et al. (2017). Hollow iron-vanadium composite spheres: a highly efficient iron-based water oxidation electrocatalyst without the need for nickel or cobalt. *Angew. Chemie-International Ed.* 56 (12), 3289–3293. doi:10.1002/anie.201611863

Fan, K., Zou, H., Duan, L., and Sun, L. (2020). Selectively etching vanadium oxide to modulate surface vacancies of unary metal-based electrocatalysts for high-performance water oxidation. *Adv. Energy Mater.* 10 (5). doi:10.1002/aenm.201903571

Guo, H., Zhang, L., Ou, D., Liu, Q., Wu, Z., Yang, W., et al. (2023). Zn-leaching induced rapid self-reconstruction of NiFe-layered double hydroxides for boosted oxygen evolution reaction. *Small* 20, e2307069. doi:10.1002/smll.202307069

Huang, L., Yang, L., Guo, S., Li, Y., Zhao, L., and Jiao, L. (2021). Influence of interlayer water molecules in Ni-based catalysts for oxygen evolution reaction. *J. Energy Chem.* 53, 316–322. doi:10.1016/j.jechem.2020.05.042

Jamesh, M., and Sun, X. (2018). Recent progress on earth abundant electrocatalysts for oxygen evolution reaction (OER) in alkaline medium to achieve efficient water splitting - a review. *J. Power Sources* 400, 31–68. doi:10.1016/j.jpowsour.2018.07.125

Karmakar, A., Karthick, K., Sankar, S. S., Kumaravel, S., Madhu, R., and Kundu, S. (2021). A vast exploration of improvising synthetic strategies for enhancing the OER kinetics of LDH structures: a review. *J. Mater. Chem. A* 9 (3), 1314–1352. doi:10.1039/d0ta09788h

Li, P., Duan, X., Kuang, Y., Li, Y., Zhang, G., Liu, W., et al. (2018). Tuning electronic structure of NiFe layered double hydroxides with vanadium doping toward high efficient electrocatalytic water oxidation. *Adv. Energy Mater.* 8 (15). doi:10.1002/aenm.201703341

Peng, L., Yang, N., Yang, Y., Wang, Q., Xie, X., Sun-Waterhouse, D., et al. (2021). Atomic cation-vacancy engineering of NiFe-layered double hydroxides for improved activity and stability towards the oxygen evolution reaction. *Angew. Chemie-International Ed.* 60 (46), 24612–24619. doi:10.1002/anie.202109938

Qian, Q., He, X., Li, Z., Chen, Y., Feng, Y., Cheng, M., et al. (2023). Electrochemical biomass upgrading coupled with hydrogen production under industrial-level current density. *Adv. Mater.* 35 (25), e2300935. doi:10.1002/adma.202300935

Saad, A., Bechambi, O., Ali, S., Mushtaq, M. A., and Yasin, G. (2023). Tunning the single-phase triggered 3D mesostructured nitride with engineering the thermal nitridation effect for zinc-air batteries. *Appl. Surf. Sci.* 639, 158226. doi:10.1016/j.apsusc.2023.158226

Saad, A., Gao, Y., Owusu, K. A., Liu, W., Wu, Y., Ramiere, A., et al. (2022b). Ternary Mo_2NiB_2 as a superior bifunctional electrocatalyst for overall water splitting. *Small* 18 (6), e2104303. doi:10.1002/smll.202104303

Saad, A., Gao, Y., Ramiere, A., Chu, T., Yasin, G., Wu, Y., et al. (2022a). Understanding the surface reconstruction on ternary W_xCoB_x for water oxidation and zinc-air battery applications. *Small* 18 (17), e2201067. doi:10.1002/smll.202201067

Sagar, P., Yogesh, K., Syed, A., Marraiki, N., Elgorban, A. M., Zaghloul, N. S. S., et al. (2022). Studies on the effect of crystalline Fe_2O_3 on OER performance of amorphous NiOOH electrodeposited on stainless steel substrate. *Chem. Pap.* 76 (11), 7195–7203. doi:10.1007/s11696-022-02382-y

Schalenbach, M., Kasian, O., Ledendecker, M., Speck, F. D., Mingers, A. M., Mayrhofer, K. J. J., et al. (2018). The electrochemical dissolution of noble metals in alkaline media. *Electrocatalysis* 9 (2), 153–161. doi:10.1007/s12678-017-0438-y

Shin, H., Xiao, H., and Goddard, I. W. A. (2018). In silicon discovery of new dopants for Fe-doped Ni oxyhydroxide ($N_{1-x}Fe_xOOH$) catalysts for oxygen evolution reaction. *J. Am. Chem. Soc.* 140 (22), 6745–6748. doi:10.1021/jacs.8b02225

Shinagawa, T., Garcia-Esparza, A. T., and Takanabe, K. (2015). Insight on Tafel slopes from a microkinetic analysis of aqueous electrocatalysis for energy conversion. *Sci. Rep.* 5, 13801. doi:10.1038/srep13801

Shvets, P., Dikaya, O., Maksimova, K., and Goikhman, A. (2019). A review of Raman spectroscopy of vanadium oxides. *J. Raman Spectrosc.* 50 (8), 1226–1244. doi:10.1002/jrs.5616

Silversmit, G., Depla, D., Poelman, H., Marin, G. B., and De Gryse, R. (2004). Determination of the V2p XPS binding energies for different vanadium oxidation states (V^{5+} to V^{0+}). *J. Electron Spectrosc. Relat. Phenom.* 135 (2-3), 167–175. doi:10.1016/j.elspec.2004.03.004

Suen, N., Hung, S., Quan, Q., Zhang, N., Xu, Y., and Chen, H. M. (2017). Electrocatalysis for the oxygen evolution reaction: recent development and future perspectives. *Chem. Soc. Rev.* 46 (2), 337–365. doi:10.1039/c6cs00328a

Suppaso, C., Pongkan, N., Intachai, S., Ogawa, M., and Khaorapapong, N. (2021). Magnetically recoverable β-$Ni(OH)_2$/γ-Fe_2O_3/NiFe-LDH composites; isotherm, thermodynamic and kinetic studies of synthetic dye adsorption and photocatalytic activity. *Appl. Clay Sci.* 213, 106115. doi:10.1016/j.clay.2021.106115

Tang, F., Liu, T., Jiang, W., and Gan, L. (2020). Windowless thin layer electrochemical Raman spectroscopy of Ni-Fe oxide electrocatalysts during oxygen evolution reaction. *J. Electroanal. Chem.* 871, 114282. doi:10.1016/j.jelechem.2020.114282

Tang, M., He, Y., Ali, A., Zhu, J., Shen, P., and Ouyang, Y. (2022). *In-situ* generate robust Fe-Ni derived nano-catalyst featuring surface reconstruction for enhanced oxygen evolution reaction. *Int. J. Hydrogen Energy* 47 (66), 28303–28312. doi:10.1016/j.ijhydene.2022.06.167

Wang, Y., Qiao, M., Li, Y., and Wang, S. (2018). Tuning surface electronic configuration of NiFe LDHs nanosheets by introducing cation vacancies (Fe or Ni) as highly efficient electrocatalysts for oxygen evolution reaction. *Small* 14 (17), e1800136. doi:10.1002/smll.201800136

Xu, Z., Ying, Y., Zhang, G., Li, K., Liu, Y., Fu, N., et al. (2020). Engineering NiFe layered double hydroxide by valence control and intermediate stabilization toward the oxygen evolution reaction. *J. Mater. Chem. A* 8 (48), 26130–26138. doi:10.1039/d0ta08815c

Yang, H., Wang, C., Zhang, Y., and Wang, Q. (2019). Green synthesis of NiFe LDH/Ni foam at room temperature for highly efficient electrocatalytic oxygen evolution reaction. *Sci. China-Materials* 62 (5), 681–689. doi:10.1007/s40843-018-9356-1

Zeng, F., Mebrahtu, C., Liao, L., Palkovits, R., and Beine, A. K. (2022). Stability and deactivation of OER electrocatalysts: a review. *J. Energy Chem.* 69, 301–329. doi:10.1016/j.jechem.2022.01.025

Zhong, H., Liu, T., Zhang, S., Li, D., Tang, P., Alonso-Vante, N., et al. (2019). Template-free synthesis of three-dimensional NiFe-LDH hollow microsphere with enhanced OER performance in alkaline media. *J. Energy Chem.* 33, 130–137. doi:10.1016/j.jechem.2018.09.005

Zhu, K., Zhu, X., and Yang, W. (2019). Application of *in situ* techniques for the characterization of NiFe-based oxygen evolution reaction (OER) electrocatalysts. *Angew. Chemie-International Ed.* 58 (5), 1252–1265. doi:10.1002/anie.201802923